Supporting Information

Effects of variation of phenylpyridinyl and di-*tert*-butyl-carbazolyl substituents of benzene on the performance of the derivatives in colour-tuneable white and exciplex-based sky-blue light-emitting diodes

Simas Macionis[1], Dalius Gudeika[1], Oleksandr Bezvikonnyi[1,2], Serhii Melnykov[3], Liliya Guminilovych[3], Jurate Simokaitiene[1], Svetlana Sargsyan[4], Rasa Keruckiene[1], Dmytro Volyniuk[1], Pavlo Stakhira[3], Juozas V. Grazulevicius[1,]*

[1] Department of Polymer Chemistry and Technology, Faculty of Chemical Technology, Kaunas University of Technology, Barsausko st. 59, LT-51423, Kaunas, Lithuania

[2] Department of Physics, Faculty of Mathematics and Natural Science, Kaunas University of Technology, Studentu st. 50, LT-51368, Kaunas, Lithuania

[3] Department of Electronic Engineering, Lviv Polytechnic National University, Stepan Bandera st. 12, 79013, Lviv, Ukraine

[4] Department of Organic Chemistry, Faculty of Chemistry, Yerevan State University, A. Manoogian 1, Yerevan 0025, Armenia

* Corresponding author. E-mail address: juozas.grazulevicius@ktu.lt (Juozas Vidas Grazulevicius).

Instrumentation

The chemical composition of synthesized compounds was investigated via ^{1}H (400 MHz) and ^{13}C (101 MHz) NMR spectroscopy, the NMR spectra were recorded with Bruker Avance III instrument. NMR samples were prepared according to general procedure: 25 mg of compound was dissolved in 0.6 ml of deuterated solvent (chloroform or acetone). Mass spectra were recorded with Waters ZQ 2000 instrument.

Thermal analysis results were obtained with TA Instruments DSC Q2000 series thermal analyzer for differential scanning colorimetry (DSC) and TA Instruments TGA Q50 instrument for thermogravimetric analysis (TGA). The sample heating rate for DSC experiments was 10 °C/min under N_2 flow, the sample heating rate for TGA experiments was 20 °C/min under N_2 flow.

Cyclic voltammetry (CV) experiments were carried out with Bio-Logic SAS and a micro-AUTOLAB Type III instruments, utilizing three-electrode system: counter electrode (CE) – platinum wire, reference electrode (RE) – argentum wire and working electrode (WE) – carbon rod, electrolyte solution (0.1 M) was prepared from tetrabutylammonium hexafluorophosphate and dry CH_2Cl_2 at room temperature. Standard ferrocene/ferrocenium (Fc/Fc^{+}) redox system was used to calibrate the potential values.

Theoretical calculations. The ground-state geometries were optimized by using the B3LYP (Becke three parameters hybrid functional with Lee-Yang-Perdew correlation)[1]functional at 6-31G (d, p) level in vacuum with the Gaussian[2] program.

Firstly, the equilibrium conformer search at the ground state was performed by using the MMFF (Molecular mechanics force fields) method, and then this geometry was used for further optimization. The vertical singlet and triplet energy values were calculated by using the energy

values at the corresponding excited state geometry. The time-dependent DFT (TD-DFT) calculations were carried out with the Gaussian 16 software package. Molecular orbitals were visualized by using Gaussview. The methodology of theoretical calculations corresponds to that of the previously published theoretical investigation of the HLCT materials [3,4].

Absorption spectra of dilute solutions of synthesized compounds (concentration 10^{-5} M) were recorded with AvaSpec-2048XL spectrophotometer. PL and PL decay spectra were recorded with Edinburgh Instruments' FLS980 spectrometer, the samples were purged with N_2 to remove oxygen. The photoluminescence quantum yield (Φ_{PL}) values were calculated according to the spectral intensities of excitation PicoQuantLDH-D-C-375 laser (excitation wavelength of 377nm) and PL emission. Phosphorescence spectra were recorded at 77K utilizing liquid nitrogen cryostat Optistat DN2 and turbomolecular pump. For films of compounds doped in Zeonex (1 wt.%) the delay for the measurements of phosphorescence spectra was 1 ms.

Charge transporting properties of vacuum-deposited films of 2tCzPy, 3tCzPy and 4tCzPy were studied by the time-of-flight (TOF) method at room temperature [5]. The sample configuration was indium tin oxide (ITO) /organic layer/Al. The thicknesses (d) of the layers of **PBCz1** and PBDPA1 were measured by ProFilm3D profilometer (**Figure S7**). A laser (EKSPLA) with a wavelength of 355 nm, the precision 6517B electrometer (Keithley), and the TDS 3032C oscilloscope (Tektronix) were used in the TOF setup. The samples were excited by the laser from the ITO side. Positive voltages (V) were applied to ITO to record hole carrier transients with visible transit times (t_{tr}) at the different electric fields (E). Hole mobilities (μ_h) of **PBCz1** and **PBDPA1** were calculated using the formula $\mu_h = d^2 / (V \times t_{tr})$.

In the OLED study, ITO substrates with sheet resistance of ~15 Ωsq^{-1} were cleaned in an ultrasonic bath, involving successive immersions in deionized water and 2-propanone for 20

minutes each, followed by warming in methanol for 10 minutes. Lastly, the glass substrates were treated with UV-ozone. The current density-voltage-luminance (J-V-L) characteristics of the devices were measured in a glovebox with a Keithley 2400 source meter and a Keithley 6485 picometer equipped with a calibrated silicon photodiode.

Figures and tables.

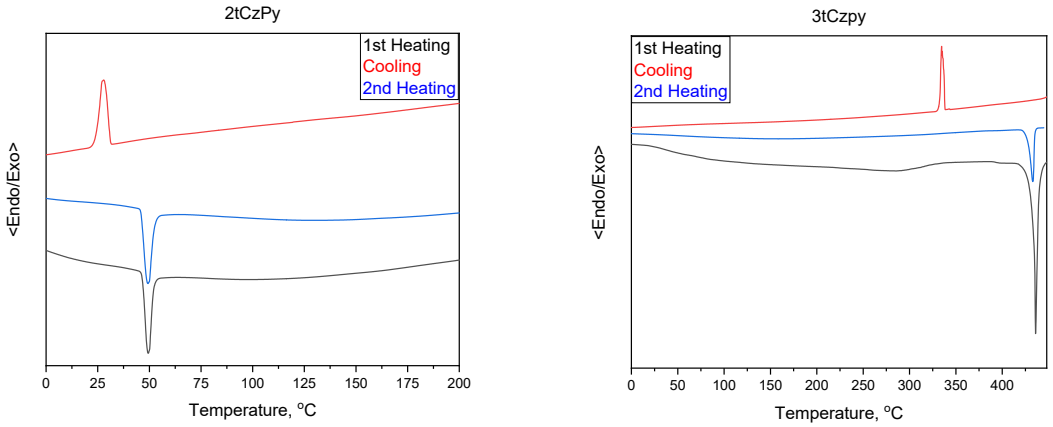

Figure S1. DSC of compounds **2tCzPy** and **3tCzPy**.

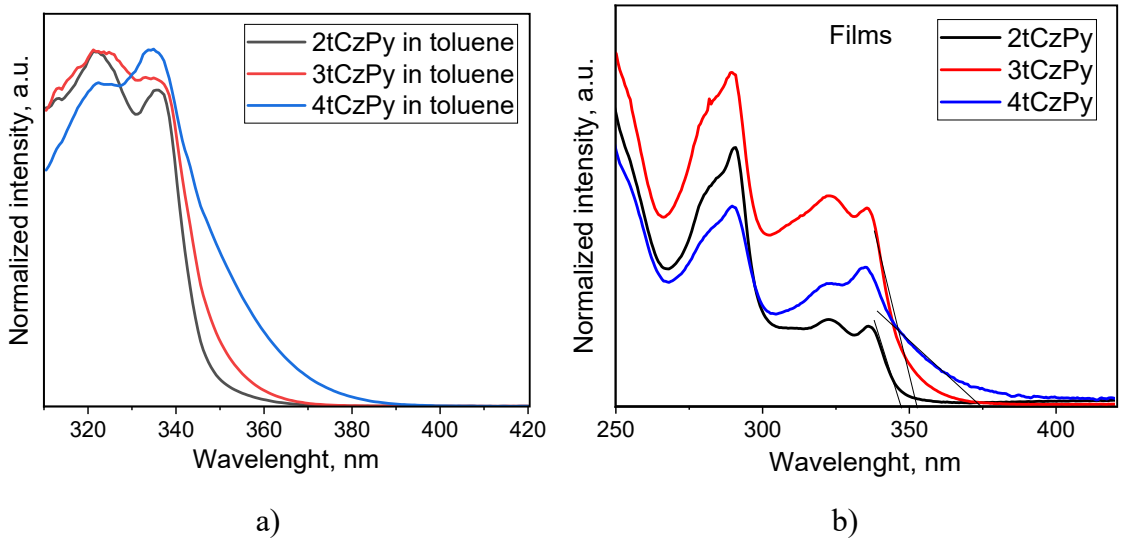

a) b)

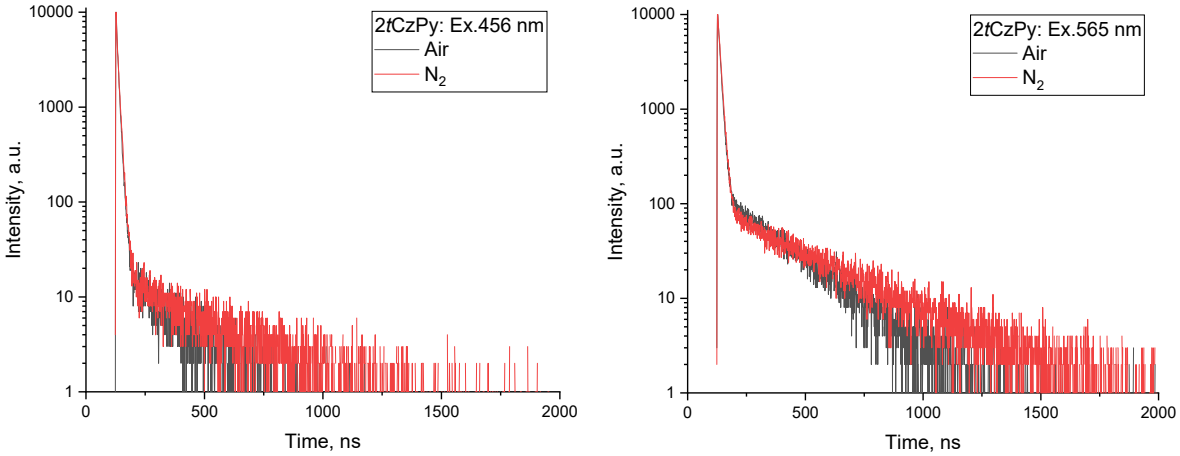

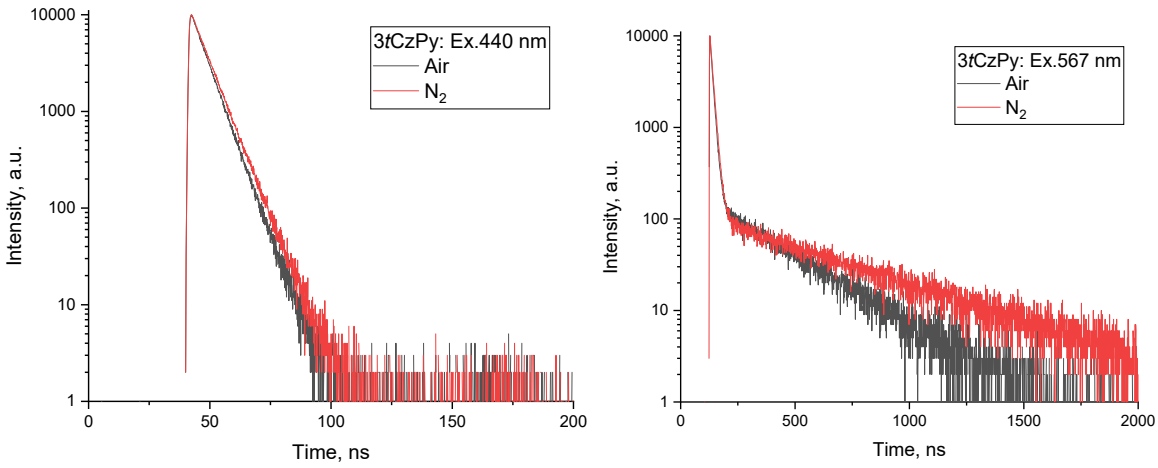
3tCzPy: Ex.440 nm
Air
N2
Intensity, a.u.
Time, ns
3tCzPy: Ex.567 nm
Air
N2
Intensity, a.u.
Time, ns

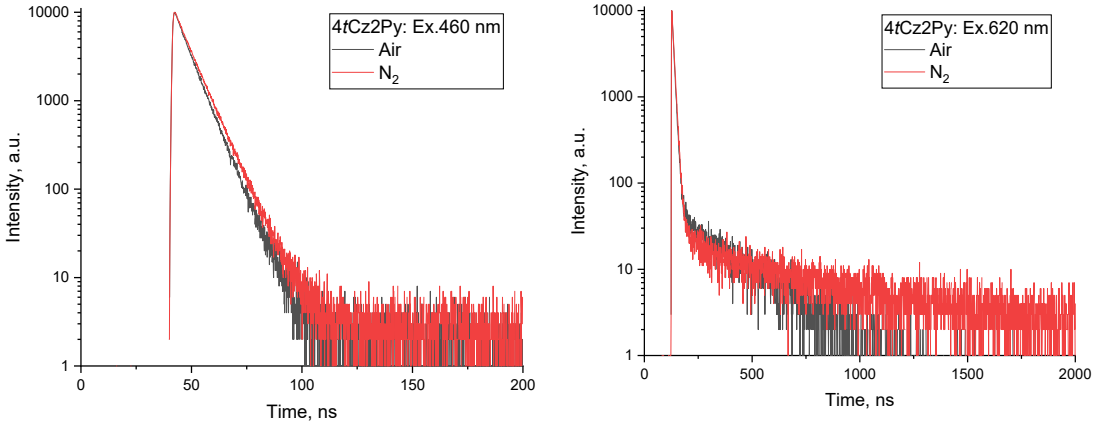
4tCz2Py: Ex.460 nm
Air
N2
Intensity, a.u.
Time, ns
4tCz2Py: Ex.620 nm
Air
N2
Intensity, a.u.
Time, ns

c)

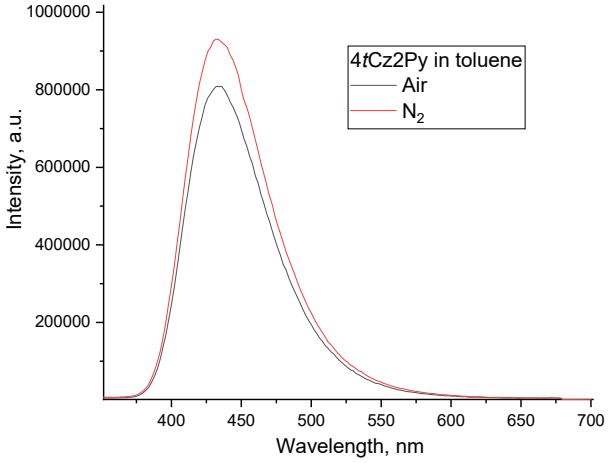
4tCz2Py in toluene
Air
N2
Intensity, a.u.
Wavelength, nm

d)

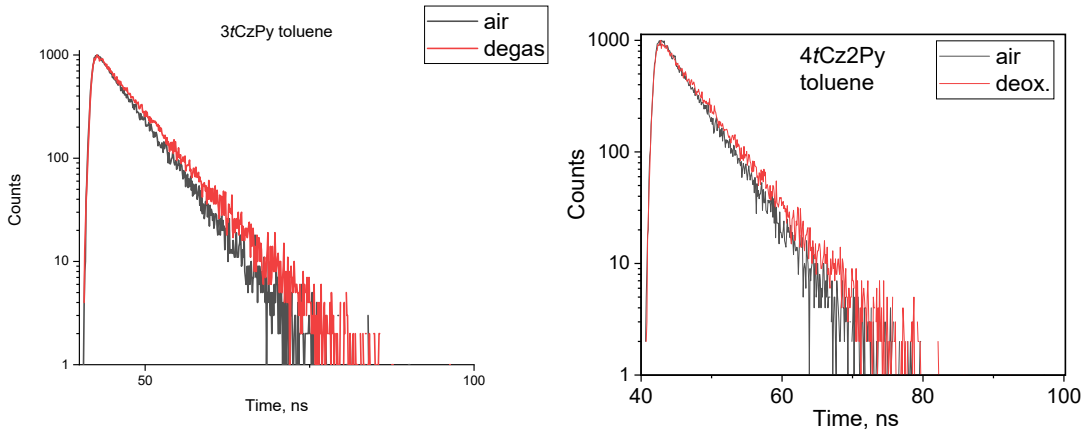

e)

Figure S2. absorption spectra of toluene solutions (a) and films (b), PL decay curves of chloroform solutions (c), PL spectra (d) and PL decay curves (e) of toluene solutions of compounds **2tCzPy**, **3tCzPy** and **4tCzPy**.

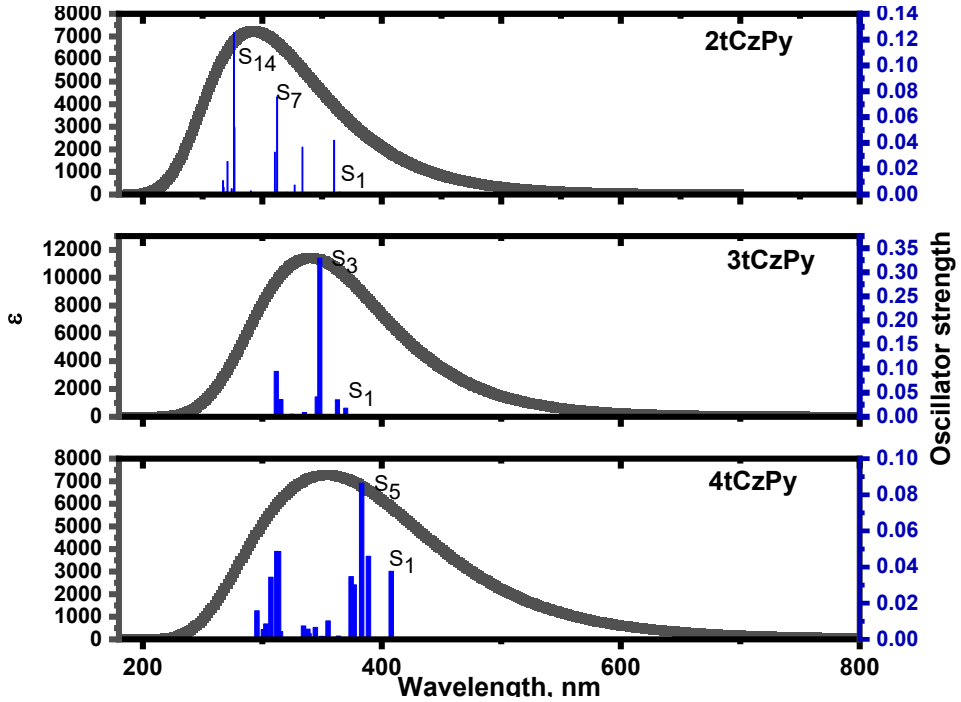

a)

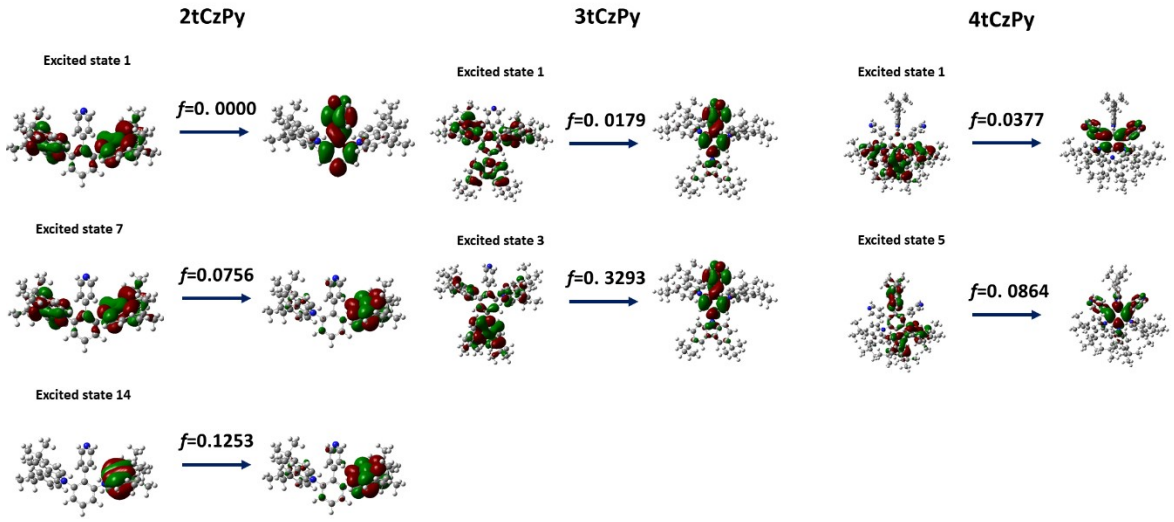

b)

Figure S3. Theoretical UV spectra (in toluene) obtained from TD-DFT calculations of compounds (a) and visualized dominating transitions (b).

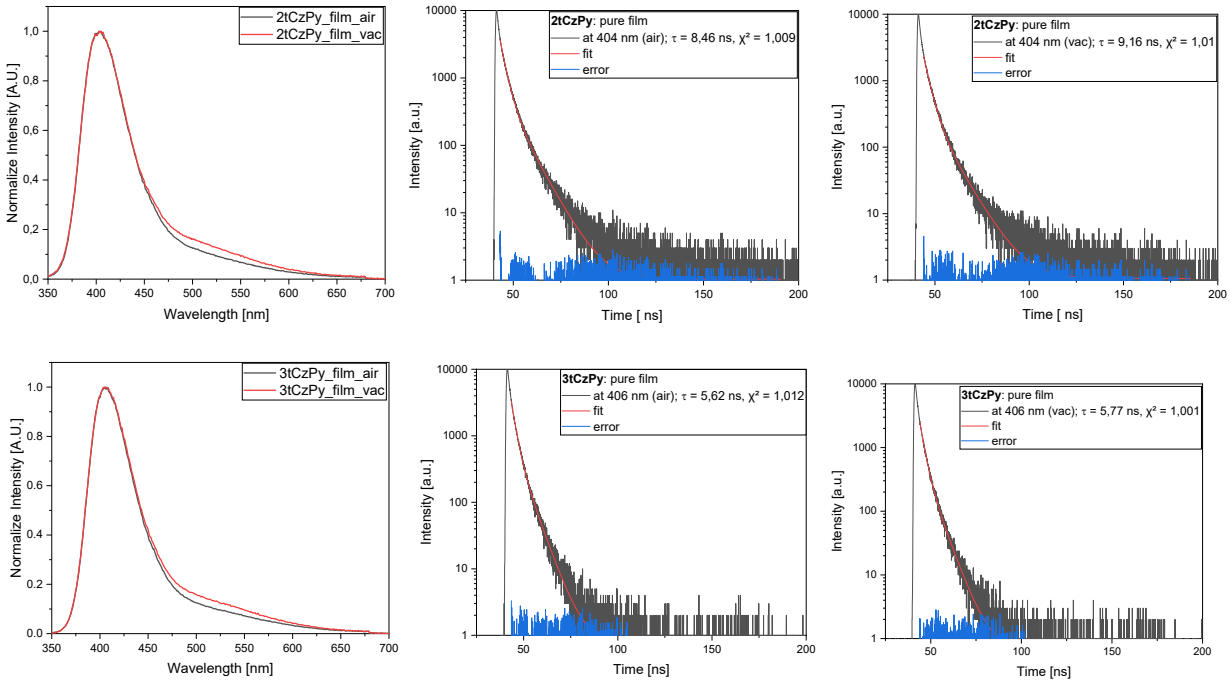

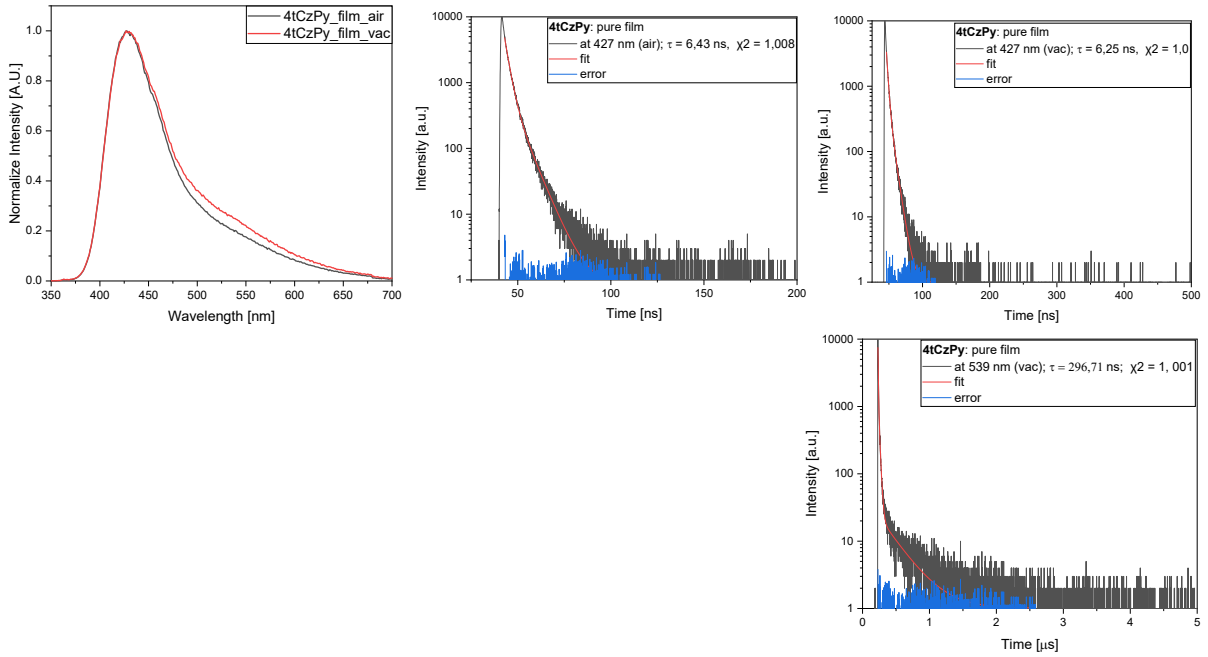

Figure S4. Normalized PL spectra (left) and PL decay curves of neat films of **2tCzPy**, **3tCzPy** and **4tCzPy** at air (center) and vacuum (right).

Table S1. Data derived from PL decay curves for neat films of **2tCzPy**, **3tCzPy** and **4tCzPy**.

Compound	**Conditions**	**Temperature, K**	**λ_{em}, nm**	**Lifetimes (τ_1, τ_2, or τ_3)**	**χ^2**
2tCzPy	Air	293	404	2.73 ns (62.84 %), 8.46 ns (37.16 %)	1.009
	Vacuum		404	3.04 ns (63.66 %), 9.16 ns (36.34 %)	1.01
3tCzPy	Air		406	2.14 ns (55.64 %), 5.62 ns (44.36 %)	1.012
	Vacuum		406	*200 ns*: 2.26 ns (56.74 %), 5.77 ns (43.26 %)	1.001
4tCzPy	Air		427	*200 ns*: 2.5 ns (63.9%), 6.43 ns (36.1 %)	1.008
	Vacuum		427	2.2 ns (64.19%), 6.34 ns (35.81 %)	1.01
	Vacuum		539	4.8 ns (53.2 %), 18.39 ns (37.12 %), 296.71 ns (9.69 %).	1.001

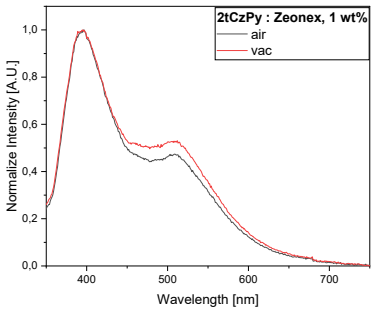
2tCzPy : Zeonex, 1 wt%
air
vac
Normalize Intensity [A.U.]
Wavelength [nm]

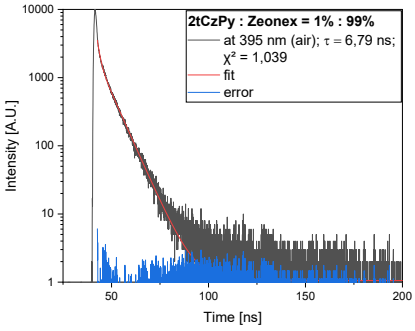
2tCzPy : Zeonex = 1% : 99%
at 395 nm (air); τ = 6,79 ns;
χ² = 1,039
fit
error
Intensity [A.U.]
Time [ns]

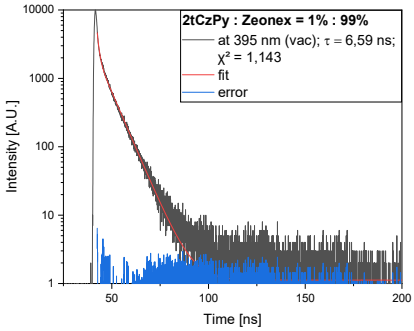
2tCzPy : Zeonex = 1% : 99%
at 395 nm (vac); τ = 6,59 ns;
χ² = 1,143
fit
error
Intensity [A.U.]
Time [ns]

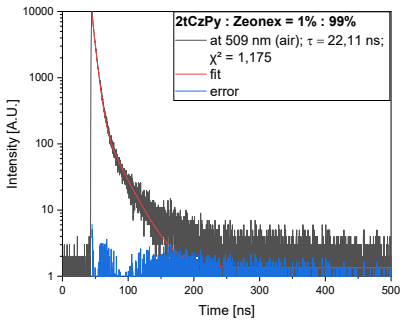
2tCzPy : Zeonex = 1% : 99%
at 509 nm (air); τ = 22,11 ns;
χ² = 1,175
fit
error
Intensity [A.U.]
Time [ns]

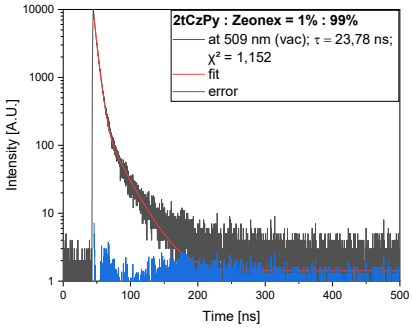
2tCzPy : Zeonex = 1% : 99%
at 509 nm (vac); τ = 23,78 ns;
χ² = 1,152
fit
error
Intensity [A.U.]
Time [ns]

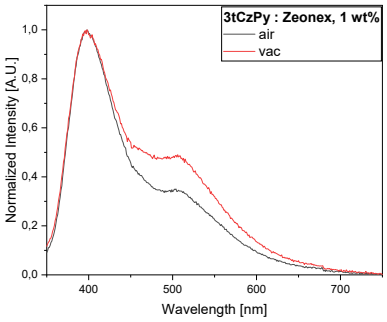
3tCzPy : Zeonex, 1 wt%
air
vac
Normalized Intensity [A.U.]
Wavelength [nm]

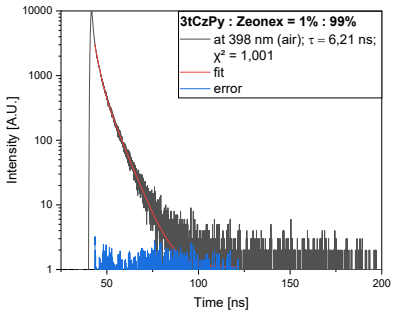
3tCzPy : Zeonex = 1% : 99%
at 398 nm (air); τ = 6,21 ns;
χ² = 1,001
fit
error
Intensity [A.U.]
Time [ns]

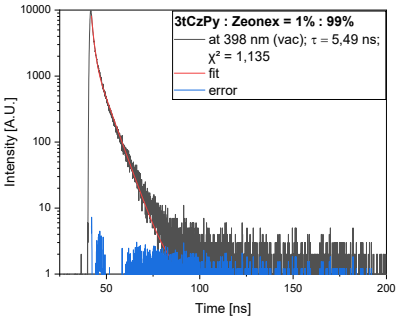
3tCzPy : Zeonex = 1% : 99%
at 398 nm (vac); τ = 5,49 ns;
χ² = 1,135
fit
error
Intensity [A.U.]
Time [ns]

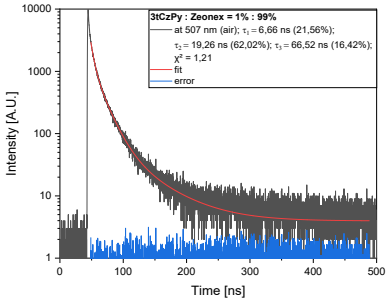
3tCzPy : Zeonex = 1% : 99%
at 507 nm (air); τ1 = 6,66 ns (21,56%);
τ2 = 19,26 ns (62,02%); τ3 = 66,52 ns (16,42%);
χ² = 1,21
fit
error
Intensity [A.U.]
Time [ns]

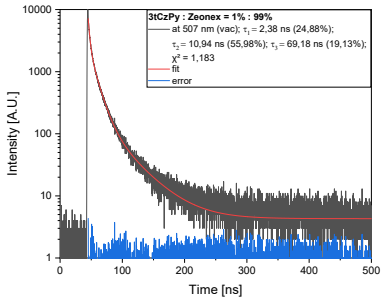
3tCzPy : Zeonex = 1% : 99%
at 507 nm (vac); τ1 = 2,38 ns (24,88%);
τ2 = 10,94 ns (55,98%); τ3 = 69,18 ns (19,13%);
χ² = 1,183
fit
error
Intensity [A.U.]
Time [ns]

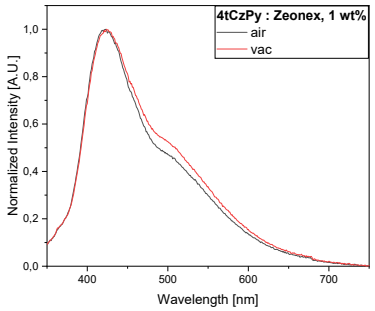
4tCzPy : Zeonex, 1 wt%
air
vac
Normalized Intensity [A.U.]
Wavelength [nm]

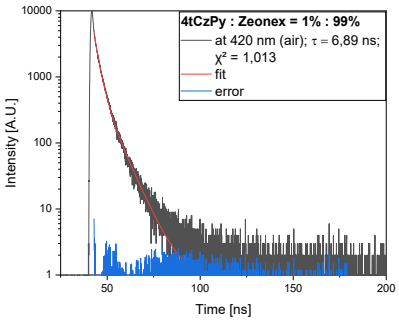
4tCzPy : Zeonex = 1% : 99%
at 420 nm (air); τ = 6,89 ns;
χ² = 1,013
fit
error
Intensity [A.U.]
Time [ns]

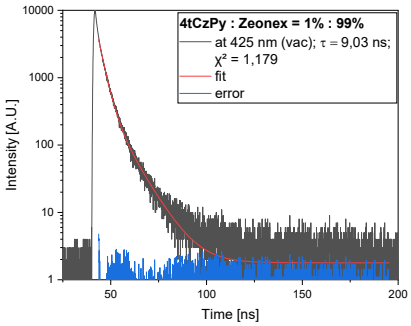
4tCzPy : Zeonex = 1% : 99%
at 425 nm (vac); τ = 9,03 ns;
χ² = 1,179
fit
error
Intensity [A.U.]
Time [ns]

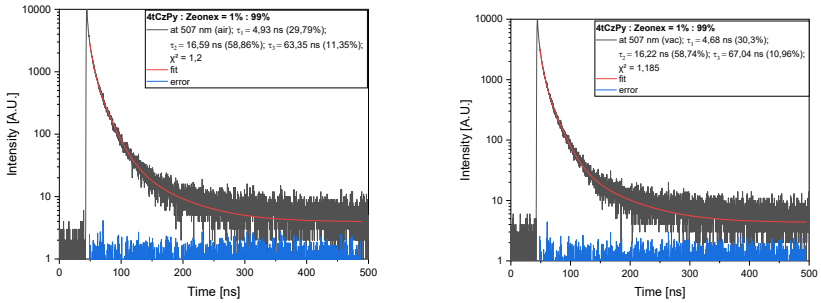

Figure S5. Normalized PL spectra (left) and PL decay curves of Zeonex-based films of **2tCzPy**, **3tCzPy** and **4tCzPy** at air (center) and vacuum (right) (compound 1 wt.% in Zeonex martix).

Table S2. Data derived from PL decay curves for Zeonex-based films of **2tCzPy**, **3tCzPy** and **4tCzPy** (compound 1 wt.% in Zeonex martix) at air and vacuum.

Compound	**Conditions**	**Temperature, K**	**λ_{max}, nm**	**Lifetimes (τ_1, τ_2, or τ_3)**	**χ^2**
2tCzPy	Air	293	395	1.34 ns (17.06 %), 6.79 ns (82.94 %)	1.039
	Air		**509**	5.32 ns (62.57 %), 22.2 ns (37.43 %)	1.195
	Vacuum		395	0.97 ns (17.19 %), 6.59 ns (82.81 %)	1.143
	Vacuum		**509**	5.43 ns (62.85 %), 23.5 ns (37.15 %)	1.185
3tCzPy	Air		398	2.08 ns (39.52 %), 6.21 ns (60.48 %)	1.001
	Air		**507**	7.24 ns (39.81 %), 23.9 ns (60.19 %)	1.185
	Vacuum		398	1.17 ns (40.97 %), 5.49 ns (59.03 %)	1.135
	Vacuum		**507**	5.93 ns (41.56 %), 22.05 ns (58.44 %)	1.185
4tCzPy	Air		420	2.36 ns (61.98 %), 6.89 ns (38.02 %)	1.013
	Air		**507**	5.77 ns (38.51 %), 20.5 ns (61.49 %)	1.197
	Vacuum		425	*200 ns*: 2.88 ns (68.56 %), 9.03 ns (31.44 %)	1.179
	Vacuum		**507**	*200 ns*: 5.48 ns (40.41 %), 20.02 ns (59.59 %).	1.175

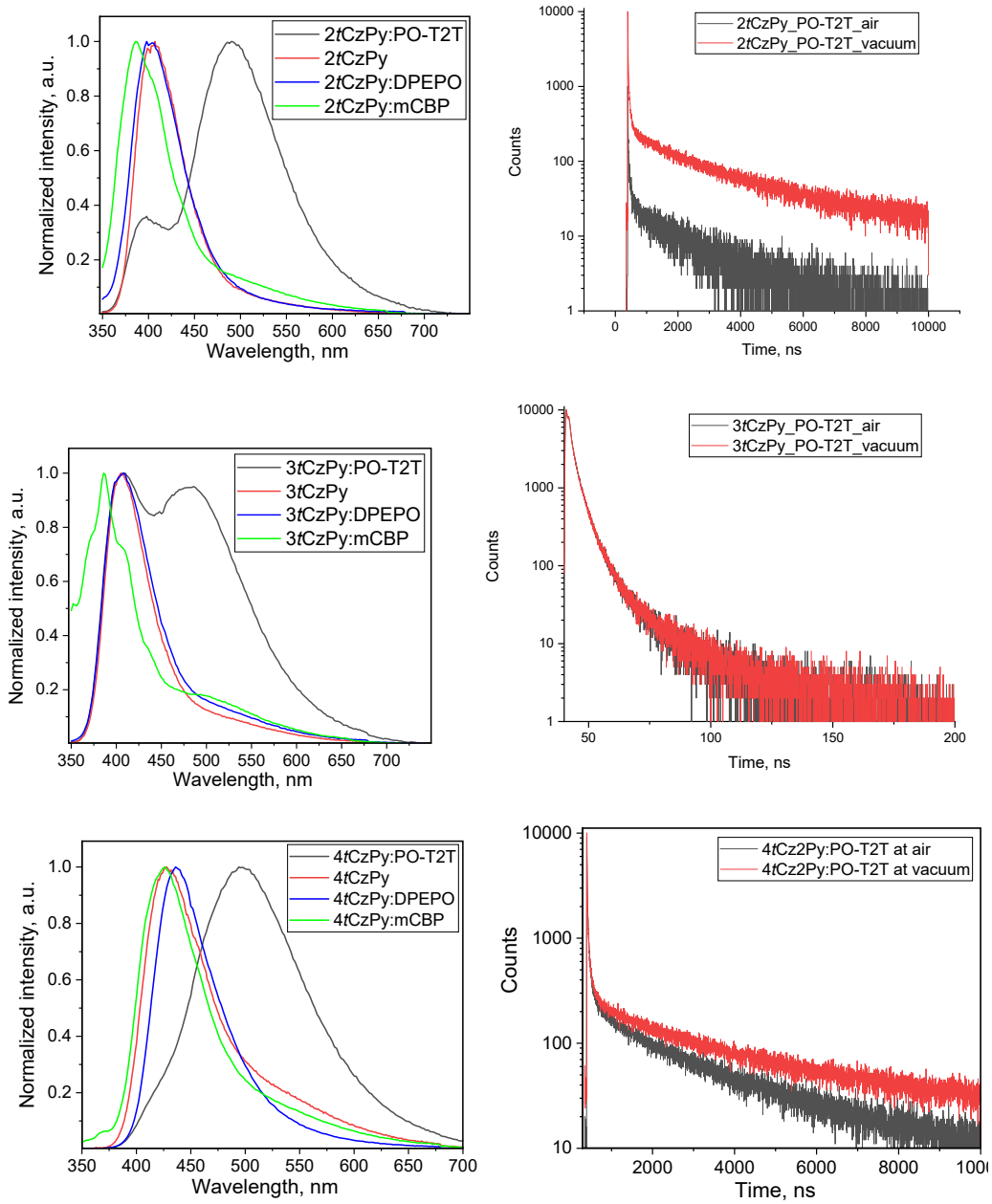

Figure S6. Normalized PL spectra (left) of films of **2tCzPy**, **3tCzPy** and **4tCzPy** and their dispersions in PO-T2T, DPEPO, or mCBP and PL decay curves of films of **2tCzPy**, **3tCzPy** and **4tCzPy** dispersed in PO-T2T at air and vacuum (compound 50 wt.% in PO-T2T).

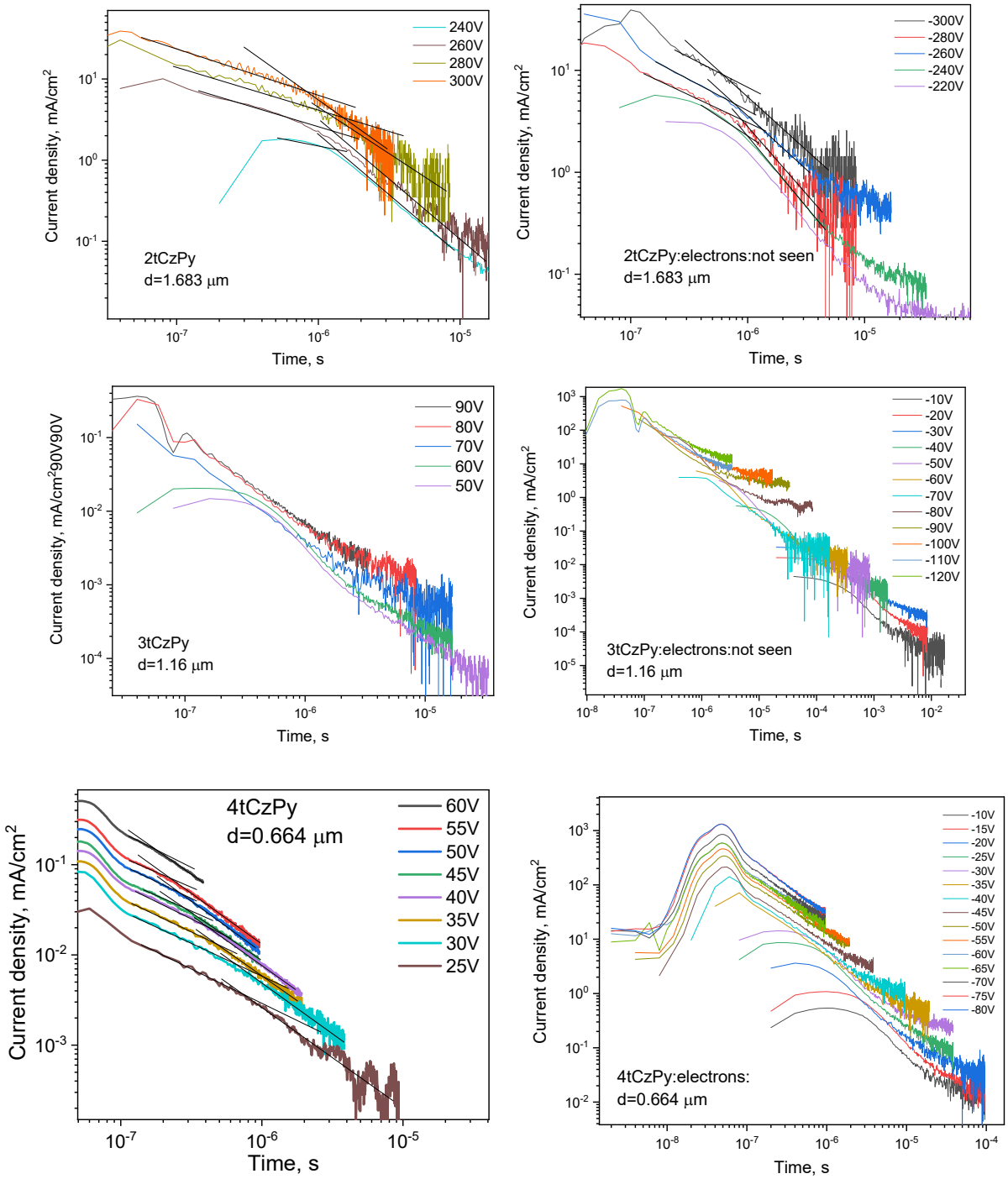

Figure S7. TOF measurements for holes and electrons in the vacuum-deposited films of **2tCzPy**, **3tCzPy** and **4tCzPy**.

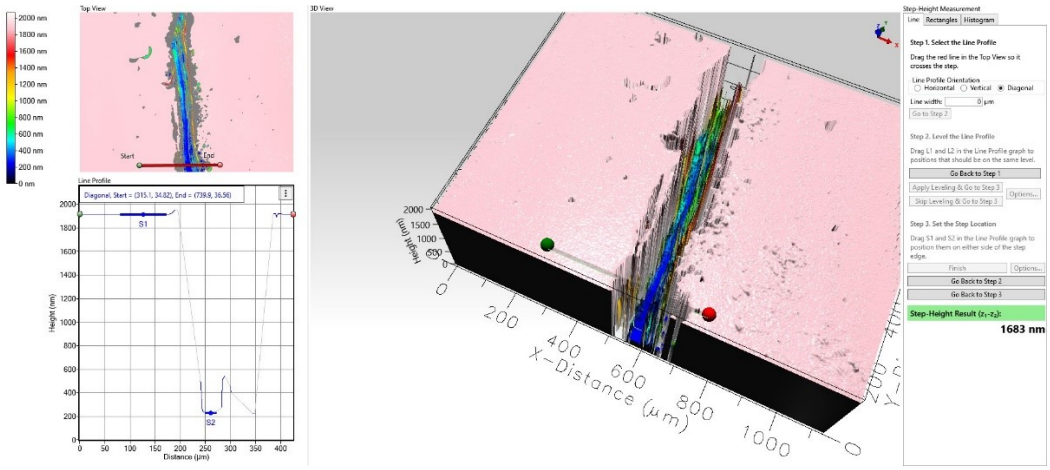

a)

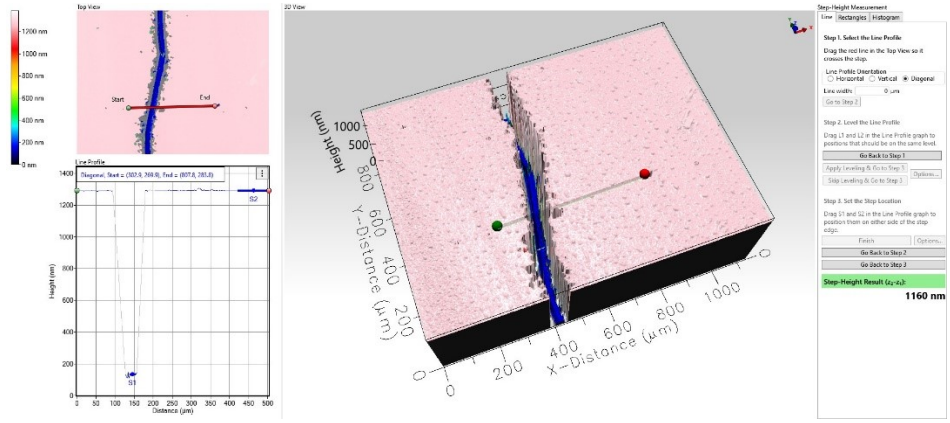

b)

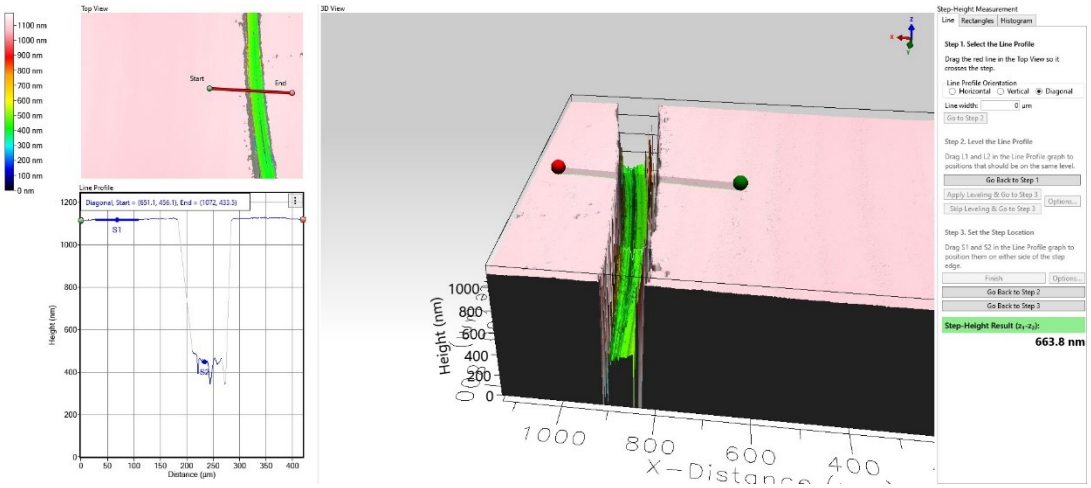

c)

Figure S8. Measurements of thicknesses of the vacuum-deposited films of **2tCzPy** (a), **3tCzPy** (b) and **4tCzPy** (c) used in the TOF measurements.

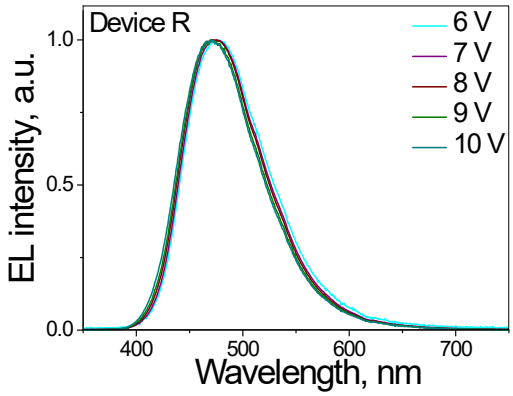

Figure S9. EL spectra of the reference device R at different voltages.

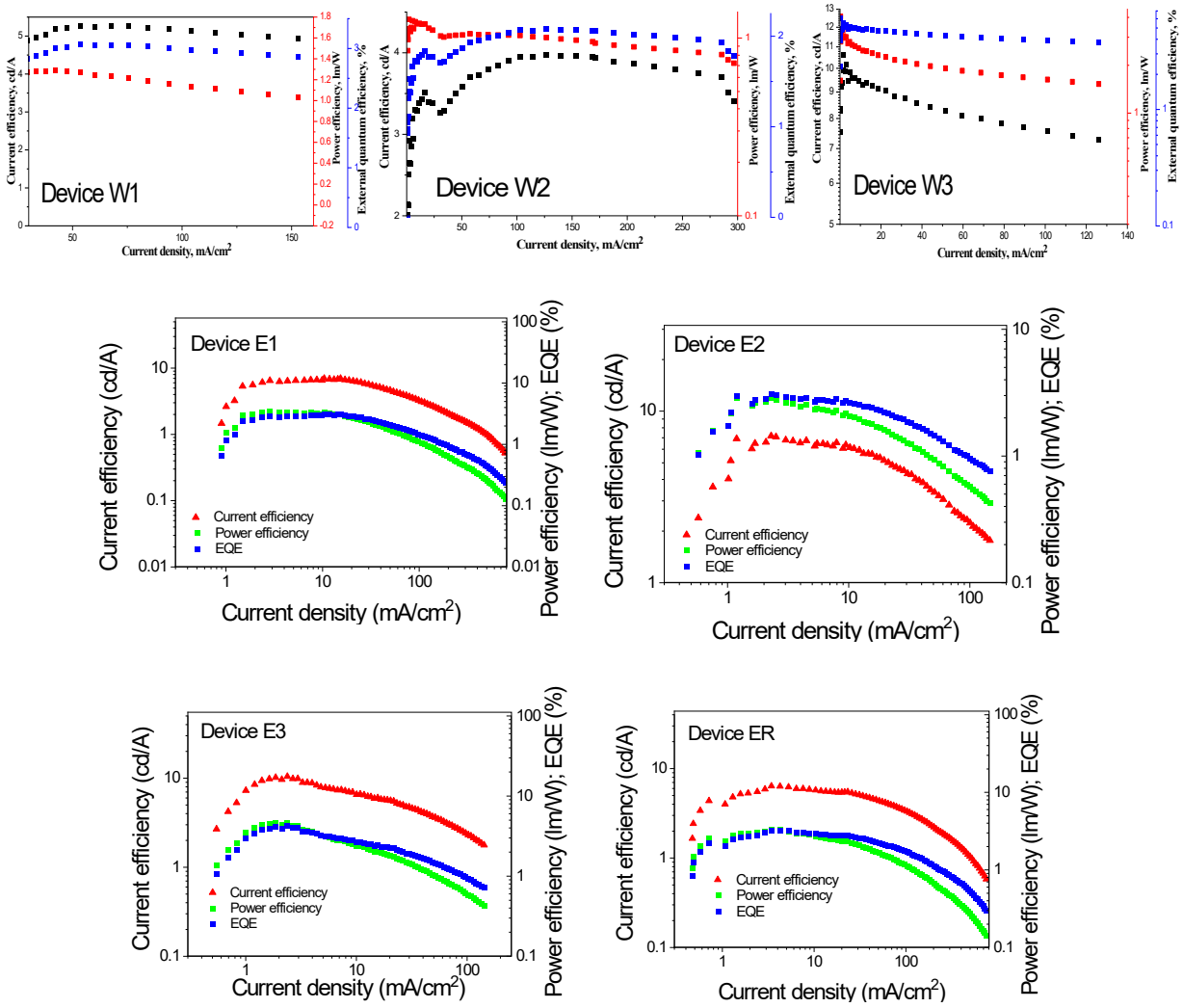

Figure S10. Current, power and EQE as the function of current density for devices W1-3, E1-3 and ER.

Electroluminescence of doping-free OLEDs.

We fabricated doping-free devices N1, N2 and N3 using **2tCzPy**, **3tCzPy**, and **4tCzPy** for the deposition of the light-emitting layers (EML), respectively. The device structure was as follows: ITO / HAT-CN (16 nm) / NPB (45 nm) / mCP (5 nm) / EML (25 nm) / TSPO1 (8 nm) / TPBi (80 nm) / LiF (0.4 nm) / Al. The exciton-blocking layers of mCP and TSPO1 were used to ensure that EL properties can be completely attributed to EML. The main EL characteristics of the devices are collected in **Figures S11** and **S12**. Device N2 did not show measurable EL because of the charge transporting issues of **3tCzPy** (**Figure 5c**). In contrast, devices N1 and N3 showed EL spectra with two bands similar to those observed in EL spectra of OLEDs W1-W3 (**Figure S11a**). The EL intensities of those bands were found to be different for devices W1-W3 and N1/N3 since DPEPO was used as a host in the case of colour-tuneable white OLEDs.

We collected EL decay curves for devices N1 and N3 (**Figure S12**). According to the EL dynamics studied at the different wavelengths, compounds emit short-lived emissions at the short wavelengths and long-lived emissions in the low-energy region. The long-lived EL of the devices is the additional evidence of triplet harvesting by the compounds.

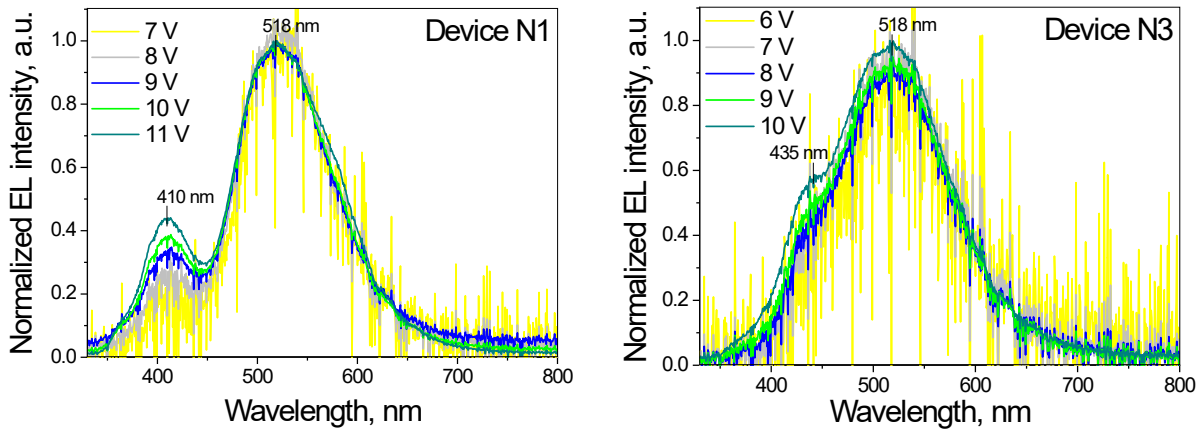

a)

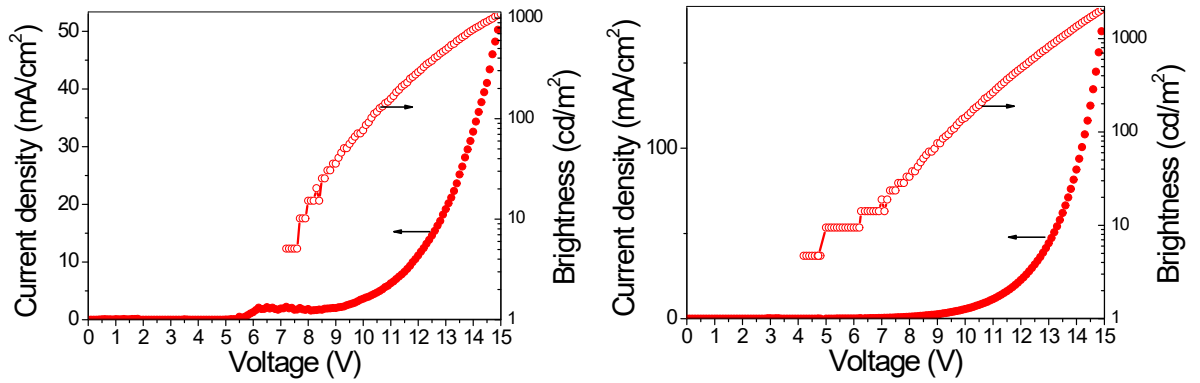

b)

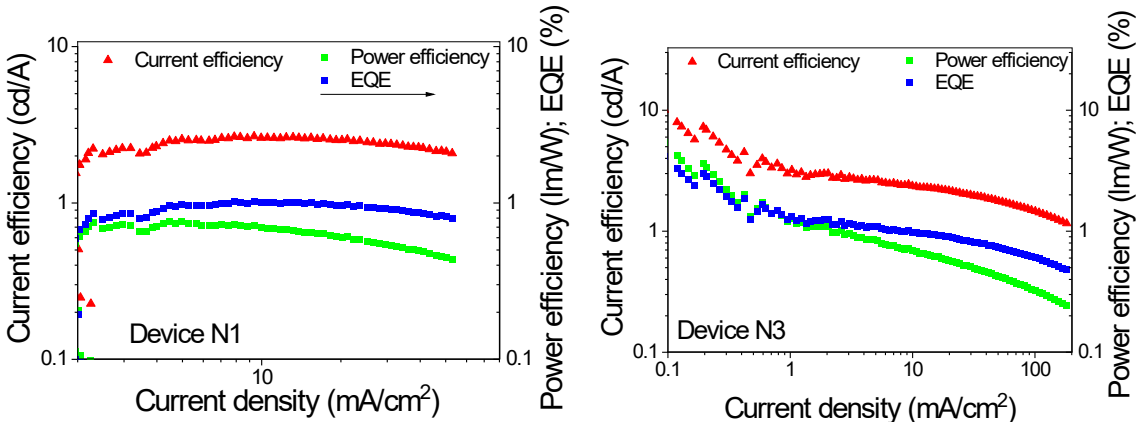

c)

Figure S11. EL spectra recorded at the different voltages (a), current density/brightness (b) versus voltage plots and current efficiency, power efficiency and EQE (c) versus current density of devices N1 and N2.

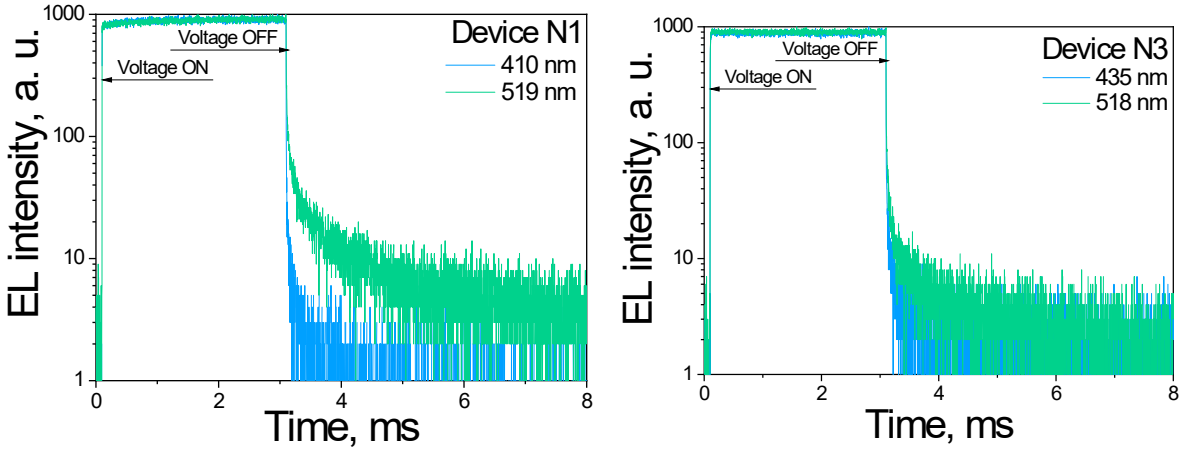

Figure S12. EL decay curves of devices N1 and N2 recorded at the different wavelengths.

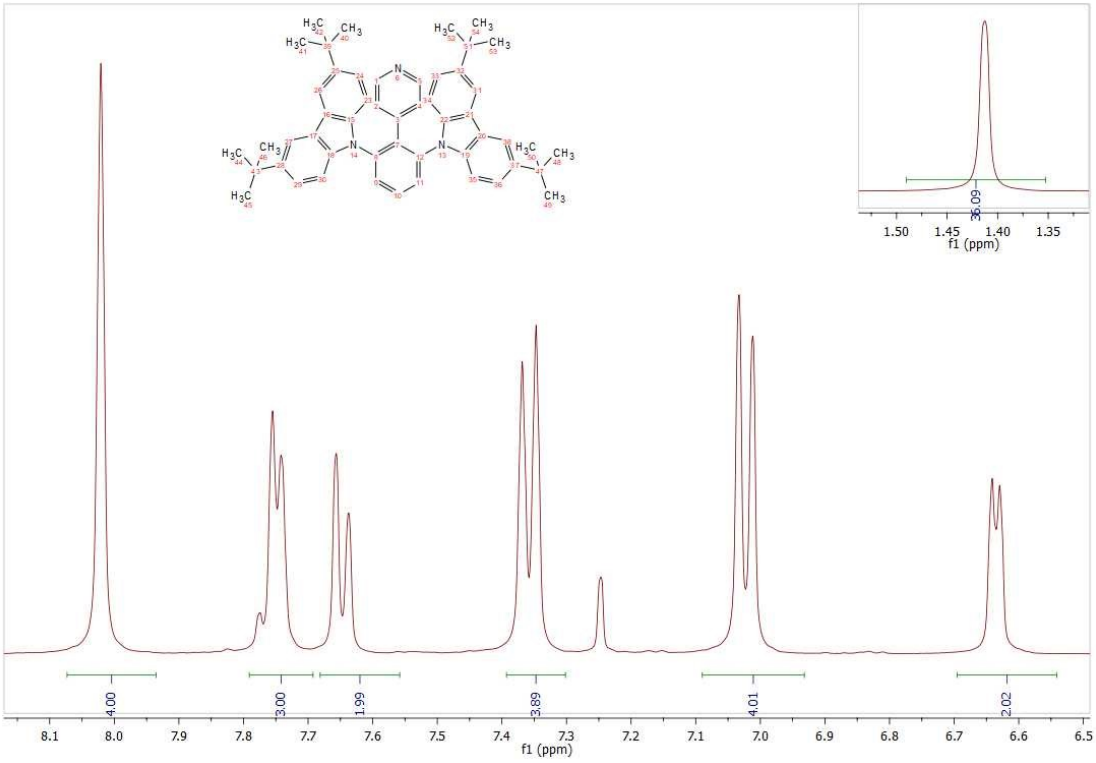

Figure S13. ^{1}H NMR spectrum of **2tCzPy** in $CDCl_3$

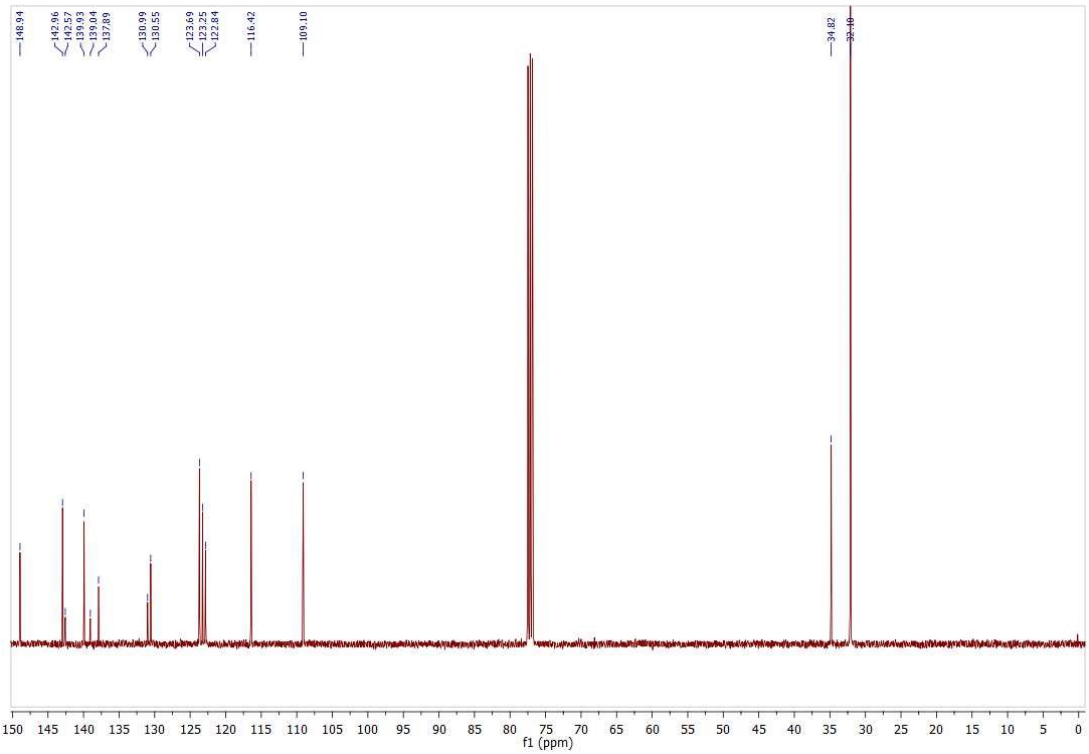

Figure S14. ^{13}C NMR spectrum of **2tCzPy** in $CDCl_3$

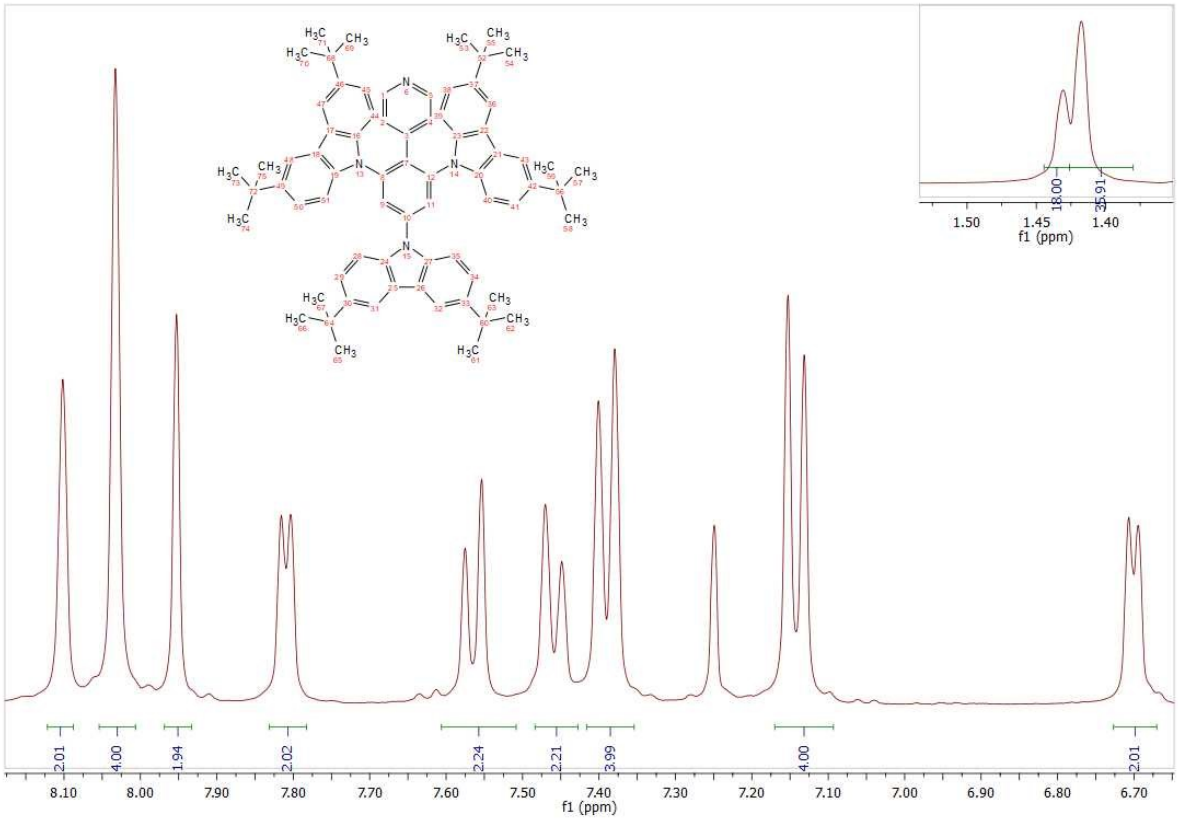

Figure S15. ^{1}H NMR spectrum of **3tCzPy** in $CDCl_3$

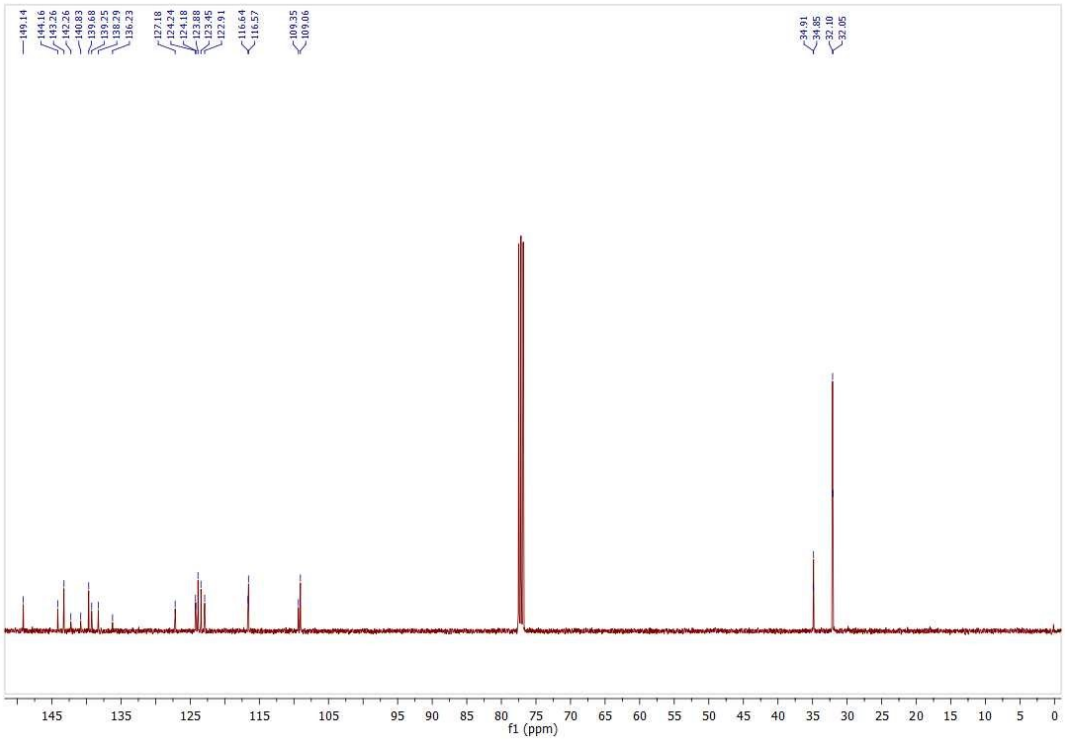

Figure S16. ^{13}C NMR spectrum of **3tCzPy** in $CDCl_3$

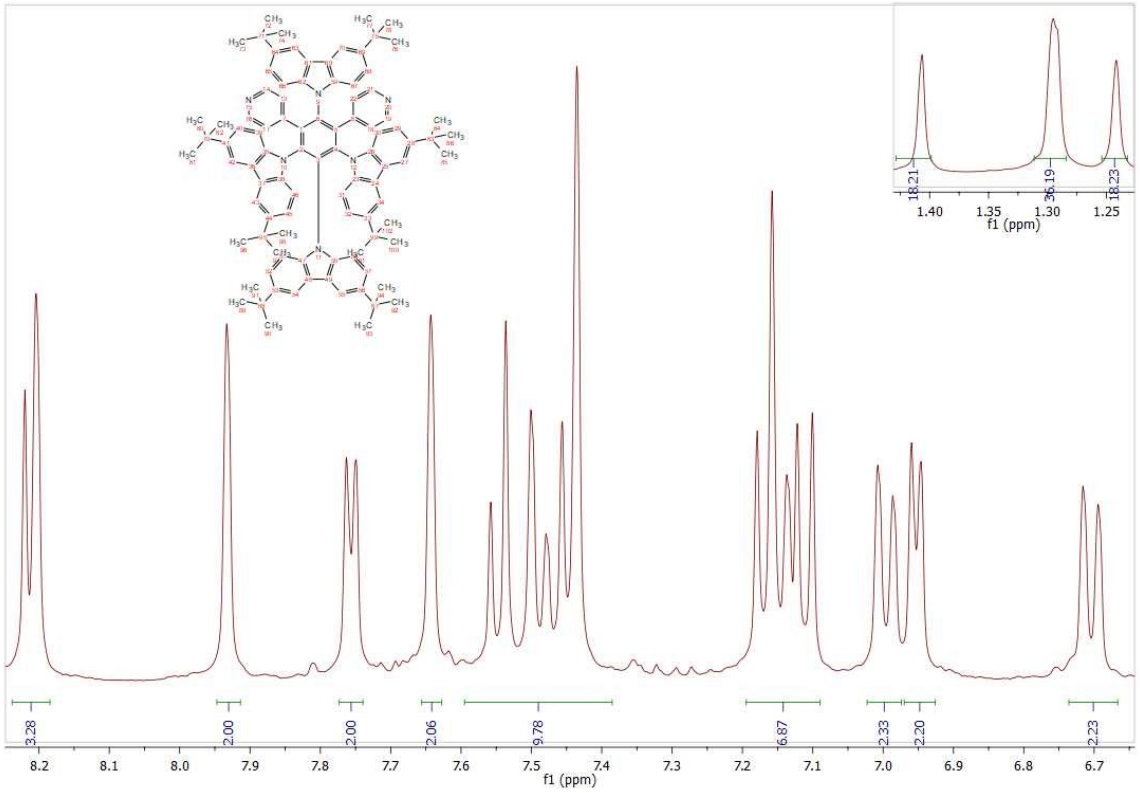

Figure S17. ^{1}H NMR spectrum of **4tCzPy** in acetone-d_6

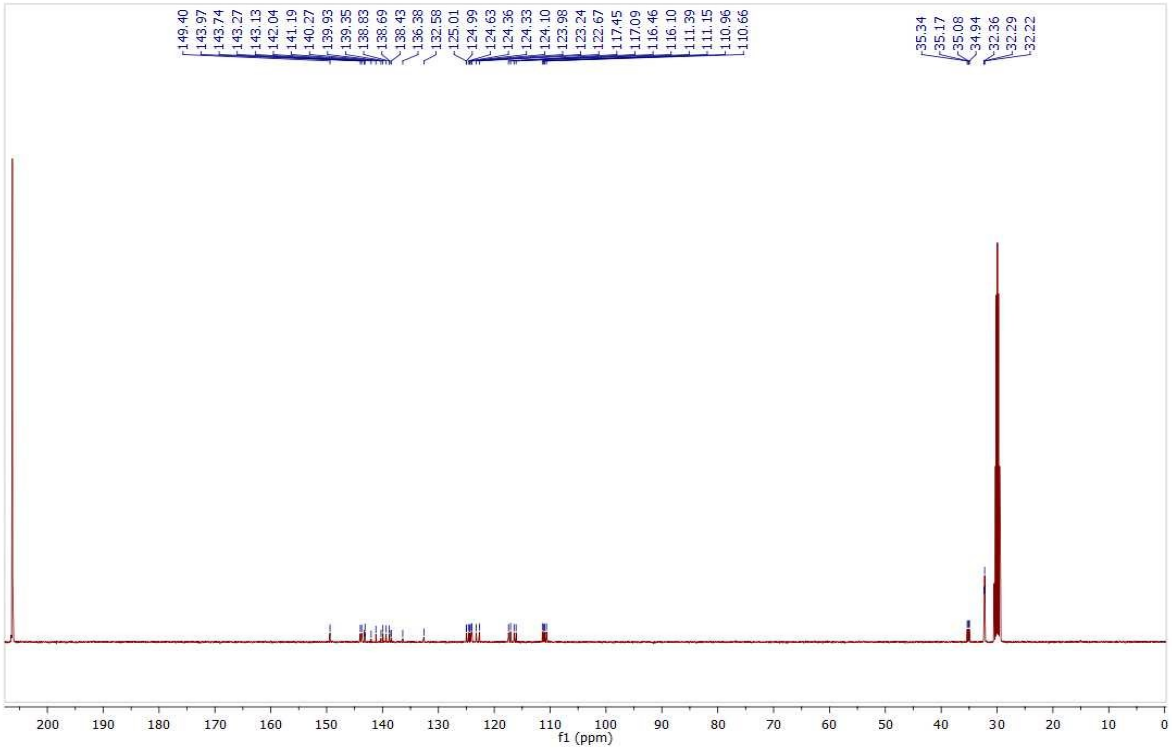

Figure S18. ^{13}C NMR spectrum of **4tCzPy** in acetone-d_6

References

1 A. D. Becke, *Phys Rev A (Coll Park)*, 1988, **38**, 3098–3100.

2 M. J. Frisch, G. W. Trucks, H. B. Schlegel, G. E. Scuseria, M. A. Robb, J. R. Cheeseman, G. Scalmani, V. Barone, G. A. Petersson, H. Nakatsuji, X. Li, M. Caricato, A. Marenich, J. Bloino, B. G. Janesko, R. Gomperts, B. Mennucci, H. P. Hratchian, J. V. Ortiz, A. F. Izmaylov, J. L. Sonnenberg, D. Williams-Young, F. Ding, F. Lipparini, F. Egidi, J. Goings, B. Peng, A. Petrone, T. Henderson, D. Ranasinghe, V. G. Zakrzewski, J. Gao, N. Rega, G. Zheng, W. Liang, M. Hada, M. Ehara, K. Toyota, R. Fukuda, J. Hasegawa, M. Ishida, T. Nakajima, Y. Honda, O. Kitao, H. Nakai, T. Vreven, K. Throssell, Jr. J. A. Montgomery, J. E. Peralta, F. Ogliaro, M. Bearpark, J. J. Heyd, E. Brothers, K. N. Kudin, V. N. Staroverov, T. Keith, R. Kobayashi, J. Normand, K. Raghavachari, A. Rendell, J. C. Burant, S. S. Iyengar, J. Tomasi, M. Cossi, J. M. Millam, M. Klene, C. Adamo, R. Cammi, J. W. Ochterski, R. L. Martin, K. Morokuma, O. Farkas, J. B. Foresman and D. J. Fox, *Gaussian, Inc. Wallingford CT*.

3 R. Keruckiene, M. Guzauskas, D. Volyniuk, D. A. da Silva Filho, G. Sini and J. V. Grazulevicius, *Spectrochim Acta A Mol Biomol Spectrosc*, 2023, **303**, 123200.

4 K. Leitonas, B. Vigante, D. Volyniuk, A. Bucinskas, R. Keruckiene, P. Dimitrijevs, T.-L. Chiu, J. V. Grazulevicius and P. Arsenyan, *J Mater Chem C Mater*, 2023, **11**, 9514–9526.

5 H. Naito, K. Tanaka, J. Singh, M. R. Narayan, D. Ompong, T. Kobayashi, T. Nagase, M. Funahashi, A. Saeki, A. S. Mishchenko, T. Manaka, M. Iwamoto, H. Matsui, Y. Noguchi, H. Ishii, L. Jäger, T. D. Schmidt, W. Brütting, L. Zhao, D. Kim, J.-C. Ribierre, T. Komino, C. Adachi, M. Uno, I. Osaka, K. Takimiya and K. Okamoto, *Organic Semiconductors for Optoelectronics*, Wiley, 2021.